Miller, W. and X. Huang. 1988. *An algorithm for searching restriction maps.* TR 88–41 Dept. of Computer Science, The Pennsylvania State University, University Park, PA 16802.
Miller, W. and E. W. Myers. 1988. Sequence comparison with concave weighting functions. *Bull. math. Biol.* **50**, 97–120.
Miller, W., J. Ostell and K. E. Rudd. 1990. An algorithm for searching restrictions maps. *CABIOS* **6**, 247–252.
Sleator, D. D. and R. E. Tarjan. 1985. Self-adjusting binary search trees. *J. ACM* **32**, 652–686.
Waterman, M. S. 1984. Efficient sequence alignment algorithms. *J. theor. Biol.* **108**, 333–337.
Waterman, M. S., T. F. Smith and H. L. Katcher. 1984. Algorithms for restriction map comparisons. *Nucl. Acids Res.* **12**, 237–242.

Revised 5 March 1991

Bulletin of Mathematical Biology Vol. 54, No. 4, pp. 619–648, 1992.
Printed in Great Britain.

0092–8240/92$5.00+0.00
Pergamon Press plc

COMPLEX DYNAMICS IN A MODEL MICROBIAL SYSTEM

MARK KOT
Department of Applied Mathematics,
University of Washington,
Seattle, WA 98195, U.S.A.

GARY S. SAYLER
Department of Microbiology,
University of Tennessee,
Knoxville, TN 37996, U.S.A.

TERRY W. SCHULTZ
Department of Animal Science–Veterinary Medicine,
University of Tennessee,
Knoxville, TN 37996, U.S.A.

The forced double-Monod model (for a chemostat with a predator, a prey and periodically forced inflowing substrate) displays quasiperiodicity, phase locking, period doubling and chaotic dynamics. Stroboscopic sections reveal circle maps for the quasiperiodic regimes and noninvertible maps of the interval for the chaotic regimes. Criticality in the circle maps sets the stage for chaos in the model. This criticality may arise with an increase in the period or amplitude of forcing.

1. Introduction. Simple models may exhibit complex dynamics. There is now an extensive literature of discrete-time (May, 1974, 1985; May and Oster, 1976; Rodgers, 1981; Kot and Schaffer, 1984, 1986; Caswell and Weeks, 1986) and continuous-time (Gilpin, 1979; May, 1980a; Inoue and Kamifukumoto, 1984; Schaffer and Kot, 1986a; Schaffer, 1985, 1989; Hastings and Powell, 1992) population models that exhibit chaotic dynamics. The empirical evidence for ecological chaos, however, is equivocal. Early work, primarily with insects (Hassell *et al.*, 1976; Stubbs, 1977; Thomas *et al.*, 1980; Bellows, 1981), hinted that chaos might be nothing more than a mathematical curiosity. In contrast, recent investigations, using Takens' (1981) lag-plot method for phase portrait reconstruction, suggest that chaos is important, especially with regards to certain childhood disease epidemics (Schaffer and Kot, 1985; Schaffer, 1985; Olsen, 1987; Kot *et al.*, 1988; Olsen *et al.*, 1988; Schaffer *et al.*, 1988; Olsen and Shaffer, 1990). There has, as a result, been considerable controversy regarding the importance of chaos in population biology (Schaffer and Kot, 1986b; Berryman and Millstein, 1989; Pool, 1989a, 1989b).

In this paper, we propose the forced double-Monod model as a useful stepping-stone in the search for ecological chaos. The model describes a protozoan predator and bacterial prey in a chemostat with an inflowing substrate that is periodically forced. The equations are accessible, yet exhibit a phase-locking route to chaos. In addition, the model lends itself to experimental verification. We discuss the behavior of the model in anticipation of the necessary laboratory tests.

2. The Unforced Double-Monod System. Let us begin by reviewing the behavior of a simpler system. A chemostat is a common laboratory apparatus used to culture microorganisms. Sterile growth medium enters the chemostat at a constant rate and the volume within the chemostat is held constant by allowing excess medium (and later, microbes) to flow out through a siphon. To this chemostat we add a heterotroph, a bacterium, that finds in the medium an abundance of all necessary nutrients but one; this last nutrient is also present, but in limiting amounts. We also add a holozoic predator, typically a protist, that feeds on the heterotroph.

The specific growth rates of bacteria (Monod, 1942, 1950) and protozoans (Proper and Garver, 1966; Curds and Cockburn, 1968) saturate at sufficiently high substrate and prey concentrations. We assume the functional response of the predator on the prey and of the prey on the substrate to be of the Monod type: predator and prey exhibit a type II functional response (Holling, 1959). By tallying the growth, depredation and washout of cells and substrate in the chemostat, we may then write (Canale, 1970):

$$\frac{dS}{dt} = D(S_i - S) - \frac{\mu_1}{Y_1}\frac{SH}{K_1 + S} \tag{1a}$$

$$\frac{dH}{dt} = \mu_1 \frac{SH}{K_1 + S} - DH - \frac{\mu_2}{Y_2}\frac{HP}{K_2 + H} \tag{1b}$$

$$\frac{dP}{dt} = \mu_2 \frac{HP}{K_2 + H} - DP \tag{1c}$$

or the dynamics within the chemostat. The state variables S, H and P represent he concentration of limiting substrate, heterotrophic prey and holozoic redator. D is the dilution rate; μ_1 and μ_2 are the maximum specific growth ates of the prey and predator (attained at infinite S and H); Y_1 is the yield of rey per unit mass of substrate; Y_2 is the biomass yield of predator per unit ass of prey; K_1 and K_2 are the half-saturation or Michaelis–Menten constants r the prey and predator.

This simple system is undoubtedly imperfect. Contois (1959), Curds and Cockburn (1968) and Bazin *et al.* (1983) have all argued for a functional response that depends on the predator as well as on the prey: predators saturate at sufficiently high prey-to-predator ratios. Fredrickson (1983) in turn has pointed out that suspension-feeding ciliates (e.g. *Tetrahymena pyriformis*) often act as "prudent predators" in that they cease to feed at low prey densities (see also Alexander, 1981). This would intimate a threshold, or possibly a functional response that is sigmoidal (e.g. Jost *et al.*'s, 1973, multiple saturation model, Holling's, 1959, type III functional response). Nisbet *et al.* (1983) have argued for including the predator's endogenous metabolism. Finally, Ratnam *et al.* (1982) have argued that wall growth is a crucial, if unfortunate, factor in any chemostat model. They propose a system that incorporates wall attachment and also Jost *et al.*'s multiple saturation model. We allow that system (1) may be flawed, but continue to work with it pending more detailed experimental investigations.

It is often easiest to analyse dimensionless equations. We therefore rescale all concentrations by the inflowing substrate concentration. In addition, we rescale the prey by its yield constant, and the predator by both yield constants. Finally, we treat the reciprocal of the dilution rate as a natural measure of time:

$$x \equiv \frac{S}{S_i} \tag{2a}$$

$$y \equiv \frac{H}{Y_1 S_i} \tag{2b}$$

$$z \equiv \frac{P}{Y_1 Y_2 S_i} \tag{2c}$$

$$\tau \equiv Dt. \tag{2d}$$

After some algebra, this yields:

$$\frac{dx}{d\tau} = 1 - x - \frac{Axy}{a + x} \tag{3a}$$

$$\frac{dy}{d\tau} = \frac{Axy}{a + x} - y - \frac{Byz}{b + y} \tag{3b}$$

$$\frac{dz}{d\tau} = \frac{Byz}{b + y} - z \tag{3c}$$

with:

$$A \equiv \frac{\mu_1}{D} \qquad a \equiv \frac{K_1}{S_i} \tag{4a}$$

$$B \equiv \frac{\mu_2}{D} \qquad b \equiv \frac{K_2}{Y_1 S_i}. \tag{4b}$$

System (3) has been studied in some detail (Canale, 1970; Butler *et al.*, 1983; Cunningham and Nisbet, 1983; Waltman, 1983; Kuang, 1989). As a system of three autonomous equations, (3) appears formidable. However, conservation of mass allows us to simplify the system. In particular, by adding equations (3a–c):

$$\dot{x}+\dot{y}+\dot{z}=1-x-y-z \tag{5}$$

we may integrate and solve for the total amount of mass in the chemostat:

$$x(\tau)+y(\tau)+z(\tau)=1+(x_0+y_0+z_0)e^{-\tau}. \tag{6}$$

Clearly, $x+y+z\to 1$ as $\tau\to\infty$. We may, in other words study the asymptotic behavior of (3) on the simplex:

$$x+y+z=1 \tag{7}$$

in the first octant (see Fig. 1). With this constraint, (3) reduces to:

$$\dot{y}=\frac{A(1-y-z)y}{a+1-y-z}-y-\frac{Byz}{b+y} \tag{8a}$$

$$\dot{z}=\frac{Byz}{b+y}-z \tag{8b}$$

an autonomous system of two, first-order, differential equations.

It is a general result of nonlinear dynamics that autonomous planar systems have limit sets no wilder than equilibria and limit cycles (Andronov *et al.*, 1966). There can be no chaos here. There are, in fact, three non-negative equilibria consistent with equations (7) and (8) (see Table 1). These correspond to: (1) washout of both predator and prey; (2) washout of the predator; and (3) coexistence, at some intermediate level, of predator, prey and substrate. The stability of these equilibria may be analysed by a straightforward local analysis (Canale, 1970; Butler *et al.*, 1983; Waltman, 1983). The results of such an analysis, summarized in Table 1, are readily interpreted. The equilibrium corresponding to washout of both predator and prey, $(x_1^*, y_1^*, z_1^*)=(1, 0, 0)$, is

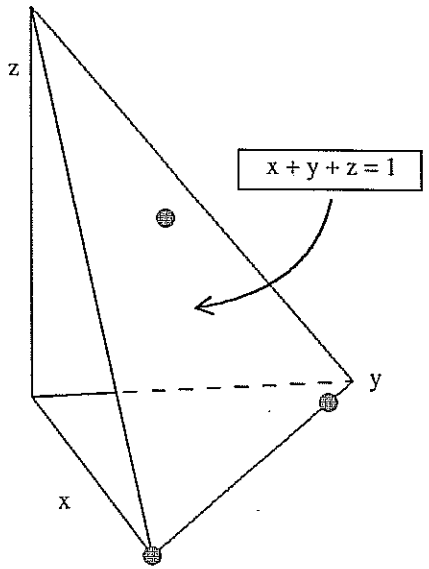

Figure 1. The simplex $x+y+z=1$ in the rescaled substrate–prey–predator phase space. Solutions of the autonomous double-Monod model tend toward this simplex in the limit of large time. There are three equilibria that occur on the simplex, corresponding to washout of both predator and prey; washout of just the predator; and coexistence of predator, prey and substrate.

stable if the prey's growth rate given a saturated substrate is still less than the washout rate, $A/(a+1)<1$. In turn, the second equilibrium is stable if the *predator* cannot invade, if the predator's growth rate at the second equilibrium is exceeded by its washout rate, $By_2^*/(b+y_2^*)<1$. The only alternative would appear to be coexistence of predator, prey and substrate at the third equilibrium. When this equilibrium is stable, it is in fact globally stable with respect to the interior of the first octant (Butler *et al.*, 1983). However, this last equilibrium may also lose stability (via a Hopf bifurcation). This bifurcation generates limit cycles and oscillations in predator, prey and substrate. Numerical simulations suggest that the limit cycles are unique and globally stable with respect to noncritical orbits in the interior of the first octant, but a complete mathematical proof to this effect is lacking (but see Kuang, 1989).

Although this broad outline is clear, details regarding the behavior of system (3) are obscured by the presence of a large number of parameters. Many of these parameters reflect physiological characteristics of the predator and prey. Fortunately, there have been a great many experimental investigations of simple microbial predator–prey systems (Proper and Garver, 1966; Salt, 1967; Curds and Cockburn, 1968; Tsuchigya *et al.*, 1972; Canale *et al.*, 1973; Jost *et al.*, 1973; van den Ende, 1973; Sudo *et al.*, 1975; Dent *et al.*, 1976; Drake and Tsuchiya, 1976, 1977; Taylor *et al.*, 1976; Curds and Bazin, 1977; Varon and

Table 1.

Location	Eigenvalues	Stability criteria
$x_1^*=1$		
$y_1^*=0$	$\lambda_1=\dfrac{A}{a+1}-1$	$\dfrac{A}{a+1}<1$
$z_1^*=0$	$\lambda_2=-1$	
$x_2^*=\dfrac{a}{A-1}$		
$y_2^*=1-\dfrac{a}{A-1}$	$\lambda_1=\dfrac{-(A-1-a)(A-1)}{aA}$	$\dfrac{A}{a+1}>1$
$z_2^*=0$	$\lambda_2=\dfrac{B(A-1-a)}{b(A-1)+(A-1-a)}-1$	$\dfrac{By_2^*}{b+y_2^*}<1$
$x_3^*=-\dfrac{1}{2}\left(a+\dfrac{Ab}{B-1}-1\right)+\dfrac{1}{2}\sqrt{\left(a+\dfrac{Ab}{B-1}-1\right)^2+4a}$	$\lambda=\dfrac{1}{2}\left[\dfrac{1-x_3^*-Ay_3^*+Ax_3^*}{a+x_3^*}-1+\dfrac{z_3^*(1-B)}{b+y_3^*}\right]$ $+\dfrac{1}{2}\left[\left(\dfrac{1-x_3^*-Ay_3^*+Ax_3^*}{a+x_3^*}-1+\dfrac{z_3^*(1-B)}{b+y_3^*}\right)^2\right.$ $\left.+4\left(\dfrac{1-x_3^*-Ay_3^*}{a+x_3^*}-1\right)\left(\dfrac{z_3^*(B-1)}{b+y_3^*}\right)\right]^{1/2}$	$\dfrac{A}{a+1}>1$ $\dfrac{By_2^*}{b+y_2^*}>1$ $\dfrac{1-x_3^*-Ay_3^*+Ax_3^*}{a+x_3^*}+\dfrac{z_3^*(1-B)}{b+y_3^*}<1$
$y_3^*=\dfrac{b}{B-1}$		
$z_3^*=1-x_3^*-y_3^*$		

Zeigler, 1978; Watson *et al.*, 1981; Graham and Canale, 1982; Ratnam *et al.*, 1982; Swift *et al.*, 1982a,b; Bazin *et al.*, 1983) and several measurements of the physiological characteristics of the attendant microbes. Cunningham and Nisbet (1983) summarize the parameters for *Colpoda steinii* and *Escherichia coli* (Proper and Garver, 1966), *Colpidium campylum* and *Alcaligenes faecalis* (Sudo *et al.*, 1975), *Tetrahymena pyriformis* and *Klebsiella aerogenes* (Curds and Cockburn, 1968), and *Tetrahymena pyriformis* and *Aerobacter aerogenes* (Canale *et al.*, 1973), and propose a generalized set of parameters that may be used in ciliate/bacterium models (see Table 2). Many of our simulations use this set of parameters.

Table 2. Generic predator–prey parameters

	Y_1 (Dimensionless)	μ_1 (h^{-1})	K_1 ($mg\,l^{-1}$)
Prey	0.4	0.5	8
	Y_2 (Dimensionless)	μ_2 (h^{-1})	K_2 ($mg\,l^{-1}$)
Predator	0.6	0.2	9

(Cunningham and Nisbet, 1983).

With a set of physiological parameters in hand, we have two parameters that remain, the dilution rate D and the inflowing substrate concentration S_i. These are, in fact, the two parameters under the control of an experimenter operating a chemostat. Table 1 may now be used to generate an operating diagram (Cunningham and Nisbet, 1983; Nisbet *et al.*, 1983) in the S_i–D parameter plane. The diagram delimits regions with different transient or asymptotic behaviors. Figure 2 illustrates an operating diagram for the generic ciliate/bacterium parameters of Cunningham and Nisbet (1983). The various regions correspond to: (a) washout of predator and prey; (b) washout of the predator; (c) coexistence at an overdamped equilibrium; (d) coexistence at an underdamped equilibrium; and (e) coexistence on a limit cycle. Figure 3 exhibits a typical phase portrait and a set of time series for case (e). The transition from (a) to (e) that occurs with an increase in S_i may be viewed as an example of the paradox of enrichment (Rosenzweig, 1971).

An operating diagram encapsulates, in a simple way, all of the interesting dynamics for the autonomous double-Monod system. This simplicity disappears as one forces the inflowing substrate. In the next section we explore how periodic forcing and the cyclicity inherent in the autonomous system may interact to yield both quasiperiodic and chaotic solutions.

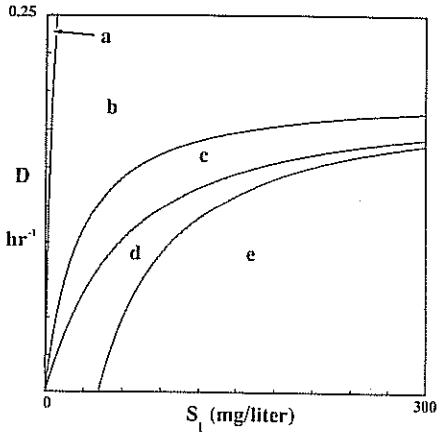

Figure 2. A typical operating diagram for the unforced double-Monod model. For various values of D, the chemostat dilution rate, and S_i, the inflowing substrate concentration, one finds five possible outcomes: (a) washout of both the predator and the prey, (b) washout of just the predator, (c) coexistence at an overdamped equilibrium, (d) coexistence at an underdamped equilibrium, and (e) coexistence on a limit cycle. After Cunningham and Nisbet (1983).

3. The Forced Double-Monod System. Natural populations are often buffeted by seasonality, diurnal cycles, or other periodic phenomena. Likewise, one can imagine a chemostat with *two* feed stocks, one nutrient-rich, one nutrient-poor, driven sinusoidally and out of phase with one another. While feed stock enters the chemostat at a constant rate, the concentration of the inflowing substrate varies periodically. System (1) is now superseded by:

$$\frac{dS}{dt} = D\left[S_i\left(1+\varepsilon \sin\frac{2\pi}{T}t\right)-S\right]-\frac{\mu_1}{Y_1}\frac{SH}{K_1+S} \tag{9a}$$

$$\frac{dH}{dt} = \mu_1\frac{SH}{K_1+S}-DH-\frac{\mu_2}{Y_2}\frac{HP}{K_2+H} \tag{9b}$$

$$\frac{dP}{dt} = \mu_2\frac{HP}{K_2+H}-DP. \tag{9c}$$

As before [equations (2)], we may rescale the variables so as to simplify our equations:

$$\frac{dx}{d\tau} = 1+\varepsilon \sin\omega\tau - x - \frac{Axy}{a+x} \tag{10a}$$

$$\frac{dy}{d\tau} = \frac{Axy}{a+x}-y-\frac{Byz}{b+y} \tag{10b}$$

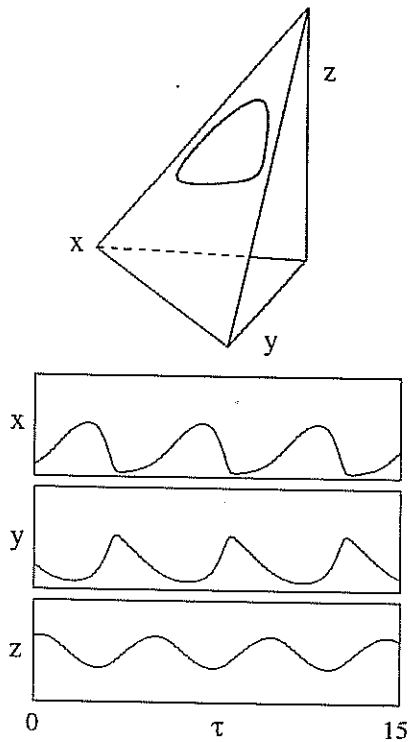

Figure 3. Phase portrait and time series illustrating a limit cycle for the unforced double-Monod model. The simulation was run with the physiological parameters of Table 2, $D=0.1\ h^{-1}$, and $S_i=115\ mg\ l^{-1}$. We illustrate: (top) a phase portrait in the rescaled substrate-prey-predator phase space; and (bottom) plots of rescaled substrate (x), prey (y) and predator (z) as a function of rescaled time (τ). Computations in this and in all subsequent simulations were performed using a fifth-order Rung–Kutta integrator with adaptive stepsize control (Press *et al.*, 1988).

$$\frac{dz}{d\tau} = \frac{Byz}{b+y}-z. \tag{10c}$$

The parameters A, a, B, and b have their previous interpretation [equation (4)] and ω is the angular frequency of the forcing in rescaled time:

$$\omega \equiv \frac{2\pi}{DT}. \tag{11}$$

Again, we utilize a first integral. Adding (10a–c):

$$\dot{x}+\dot{y}+\dot{z} = 1+\varepsilon \sin\omega\tau - x - y - z \tag{12}$$

we integrate and solve for the total mass in the chemostat:

$$x(\tau)+y(\tau)+z(\tau)=1+\frac{\varepsilon}{\sqrt{1+\omega^2}}\sin(\omega\tau-\phi)+ce^{-\tau} \tag{13}$$

where:

$$\phi=\tan^{-1}\omega. \tag{14}$$

Clearly:

$$x+y+z\to 1+\frac{\varepsilon}{\sqrt{1+\omega^2}}\sin(\omega\tau-\phi) \tag{15}$$

as $\tau\to\infty$. In this way, we may eliminate a variable and reduce the dimension of the problem. Equation (15) also provides us with an important geometric viewpoint: in the absence of forcing, the state variables may run around a limit cycle that lies on a simplex (Fig. 3). Forcing causes the entire simplex to oscillate back and forth (Fig. 4) with, in general, some different frequency.

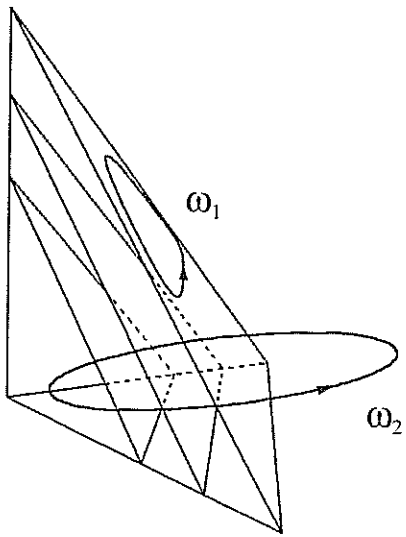

Figure 4. A schematic of the effects of forcing. In the absence of forcing, solutions may converge toward a limit cycle that lies on a simplex. Periodic forcing causes the entire simplex to oscillate back and forth. The forcing frequency and limit cycle frequency are typically incommensurate.

How will these two oscillations interact? The frequency of the simplex oscillation is that of the forcing, it's amplitude varies with the amplitude of forcing and also, rather strongly, with the angular frequency of forcing. It might be imagined that different choices of the frequency and amplitude of forcing will

lead to markedly different behaviors. This is indeed the case. Let us begin with the physiological parameters of Cunningham and Nisbet (1983) and with the chemostat parameters set to $S_i=115\ \text{mg l}^{-1}$ and $D=0.1\ \text{h}^{-1}$ so that the system exhibits a simple limit cycle (Fig. 3) of period just over 47 h ($\tau\approx 4.73$). Let us now force the system at an intermediate amplitude ($\varepsilon=0.6$) and with a relatively short period of 5 h ($\omega=4\pi$). The high angular frequency of forcing must, by equation (15), generate small amplitude oscillations of the simplex plane. The system perceives the forcing as a small perturbation of the underlying limit cycle, solutions run around a flattened torus in phase space (Fig. 5). The frequency of the limit cycle and of the forcing are incommensurate

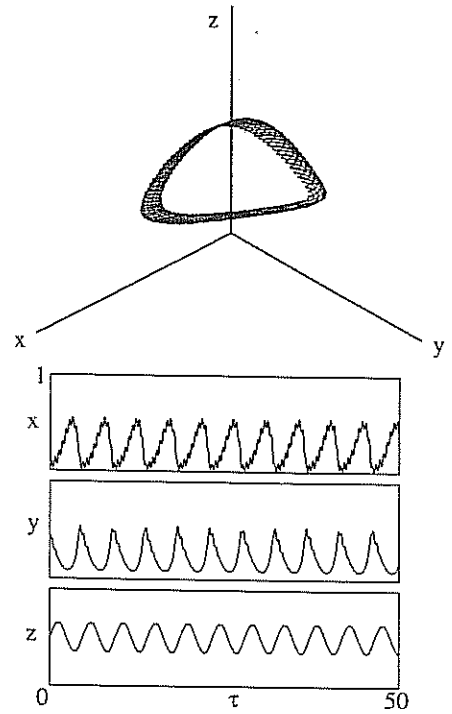

Figure 5. Quasiperiodic flow on a torus. The addition of high-frequency ($\omega=4\pi$ or $T=5$ h), intermediate-amplitude ($\varepsilon=0.6$) forcing of the substrate, for parameters otherwise identical to those in Fig. 3, yields quasiperiodic solutions that run around a torus in the rescaled substrate–prey–predator phase space. The figure illustrates: (top) a phase portrait in the rescaled substrate–prey–predator phase space; and (bottom) plots of rescaled substrate (x), prey (y), and predator (z) as a function of rescaled time (τ).

and the motion is quasiperiodic. It is worth pointing out, as an aside, an interesting trophic effect at work in Fig. 5: the perturbation is felt most strongly at the level of the substrate. As one goes up the food chain, the species do a better and better job of averaging or integrating over the perturbations.

As we increase the period of forcing it is not unusual to see periodic solutions re-emerging via frequency or mode locking. Additional increases in the period of forcing may lead to a sequence of period-doubling bifurcations and, in some cases, to chaotic solutions. A typical chaotic trajectory ($\varepsilon=0.6$, $T=24$ h) is shown in Fig. 6. The time series for the substrate and two species are aperiodic

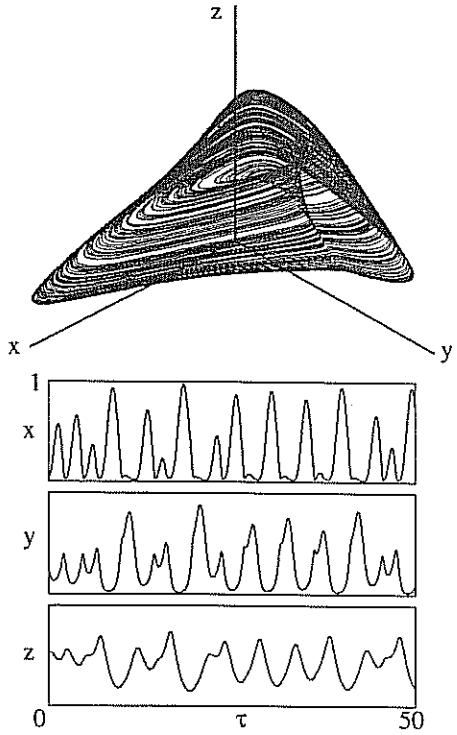

Figure 6. Chaos in the chemostat. The addition of low-frequency ($\omega=5\pi/6$ or $T=24$ h), intermediate-amplitude ($\varepsilon=0.6$) forcing of the substrate, for parameters otherwise identical to those in Fig. 3, yields solutions that run around a strange attractor in the rescaled substrate–prey–predator phase space. The figure illustrates: (top) a phase portrait in the rescaled substrate–prey–predator phase space; and (bottom) plots of rescaled substrate (x), prey (y), and predator (z) as a function of rescaled time (τ).

and rather wild. The corresponding phase portrait consists of a rather striking strange attractor. This attractor, though strange, is hardly preternatural: strange attractors appear in at least four other periodically-forced predator–prey models (Inoue and Kamifukumoto, 1984; Leven *et al.*, 1987; Schaffer, 1989; Allen, 1990).

4. A Tale of Two Maps. What are we to make of the transition from quasiperiodicity to chaos in the forced double-Monod system? Traditional time series analyses, such as spectral analysis, may be of some help in

distinguishing quasiperiodic and chaotic behavior (Glazier and Lichaber 1988). And yet, power spectra may be ambiguous. They also provide litt insight into the mechanisms underlying the transitions that we observe. Fo our purposes, Poincaré sections (Poincaré, 1892) are a better tool.

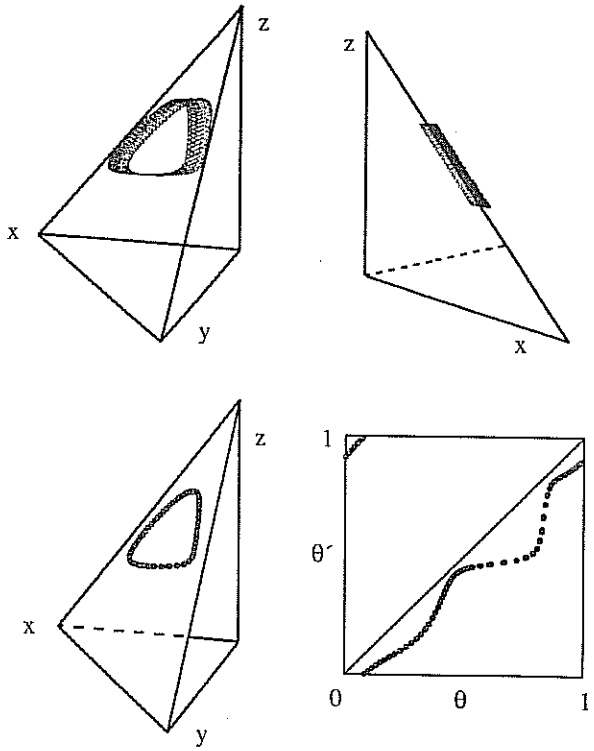

Figure 7. Section and map for quasiperiodic flow on a torus. A (top) slice with a simplex of the quasiperiodic orbit of Fig. 5 yields (bottom left) points on a curve diffeomorphic to a circle. The (bottom right) return map, a circle map, prescribes the angle of a point of intersection in terms of the angle of its predecessor. Angles have been normalized 0–1.

Poincaré sections. A Poincaré section is a sequence of points in phase space generated by the intersection of a continuous trajectory with a surface transverse to the flow (see Fig. 8). By concentrating on the points of intersection, we sacrifice continuity in time but are able to reduce the dimension of the problem. That is, we concentrate on the lower dimensional Poincaré or first return map that carries one point of intersection to the next. For a periodically forced system it is particularly easy to take a Poincaré section: we need only sample the system at one particular phase of the forcing function. In effect, we may sample the variables stroboscopically, at multiples of the forcing period.

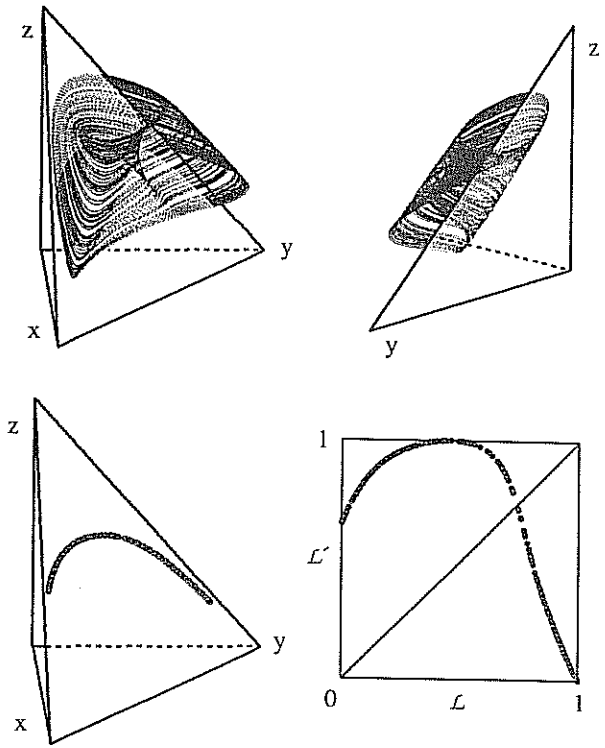

Figure 8. Section and map for a strange attractor. A (top) slice with a simplex of the chaotic orbit of Fig. 6 yields (bottom left) points on a curve diffeomorphic to a line interval. The (bottom right) return map, a noninvertible and unimodal map of the interval, prescribes the arc length to a point along the Poincaré section in terms of the arc length to its predecessor. Arc lengths have been normalized 0–1.

Stroboscopically sampling the forced double-Monod system is equivalent, by equation (15), to taking a simplex for one's surface of section. We use the two approaches, slicing our trajectories with a simplex and stroboscopically sampling the variables, interchangeably. For the quasiperiodic orbit of Fig. 5, the Poincaré section (Fig. 7) yields points that lie on a closed curve diffeomorphic to a circle. This curve may be parametrized by angle, normalized 0–1. Identifying 0 and 1, we tally the angle and the order of arrival of each point of intersection and construct a one-dimensional circle map as our return map. This return map prescribes the angle of a point of intersection in terms of the angle of its predecessor. In contrast, a slice (Fig. 8) through the strange attractor of Fig. 6 yields points that lie on a curve diffeomorphic to a line interval. We parametrize this curve by arc length, again normalized 0–1, and construct the associated return map. This unimodal return map, shown at the bottom right of Fig. 8, specifies the arc length to a point of intersection in terms of the arc length to its predecessor. In each case we are able to collapse the

dynamics of the system to that of a one-dimensional map. However, for the quasiperiodic trajectory it is an invertible map of the circle; for the chaotic trajectory, it is a noninvertible map of the interval. Each of the two maps betokens a different range of dynamics. In addition, circle maps and unimodal maps of the interval have been studied in their own right; the behavior and bifurcations found in these theoretical studies are an augur of the dynamics to be found in the forced double-Monod system.

Unimodal maps of the interval. Many biologists are familiar with unimodal maps of the interval. Maps such as the discrete-time logistic equation (Maynard Smith, 1968; May, 1972) and the Ricker curve (Ricker, 1954) may chronicle the growth of populations with discrete, nonoverlapping generations and density-dependent regulation. These maps are also the simplest dynamical systems to exhibit a sequence of bifurcations leading to chaos (May, 1974, 1976; Li and Yorke, 1975; Guckenheimer *et al.*, 1976; May and Oster, 1976; Collet and Eckmann, 1980; Devaney, 1986). As one augments a parameter, a simple equilibrium (corresponding to a limit cycle of period T for the suspended continuous-time system) loses stability to a two-cycle (period $2T$ limit cycle). Further increases in the parameter cause the two-cycle to undergo its own period-doubling bifurcation. By continuing to increase the parameter, we foment an infinite sequence of period-doublings. This sequence converges, yielding a chaotic orbit. Thereafter, chaotic and periodic orbits are both found (for different parameter values). New periodic orbits arise via tangent bifurcations and are lost through new sequences of period-doubling bifurcations. Investigators have examined the order in which the periodic orbits appear (Sarkovskii, 1964; Metropolis *et al.*, 1973; Stefan 1977), the relative abundance of periodic and chaotic orbits (Jacobson, 1981; Farmer, 1985), and regularities (Feigenbaum, 1978, 1979, 1983) and irregularities (Grebogi *et al.*, 1983) of the changes. The behaviors observed for simple unimodal maps carry over to the forced double-Monod system.

A model circle map. Even greater insight is achieved from a study of circle maps. As with unimodal maps, there is a paradigmatic example, the *standard circle* or *sine map* (Arnol'd, 1965):

$$\theta_{n+1} = f(\theta_n) \equiv \theta_n + \Omega - \frac{K}{2\pi}\sin(2\pi\theta_n) \pmod 1 \qquad (16)$$

that has been studied extensively (Jensen *et al.*, 1983, 1984; Bak, 1986; Glazier and Libchaber, 1988). This map can be iterated graphically (Fig. 9). Starting with some initial angle θ_0, we are interested in the asymptotic behavior of the orbit based at θ_0. To describe this behavior, we suspend the mod 1 action of the

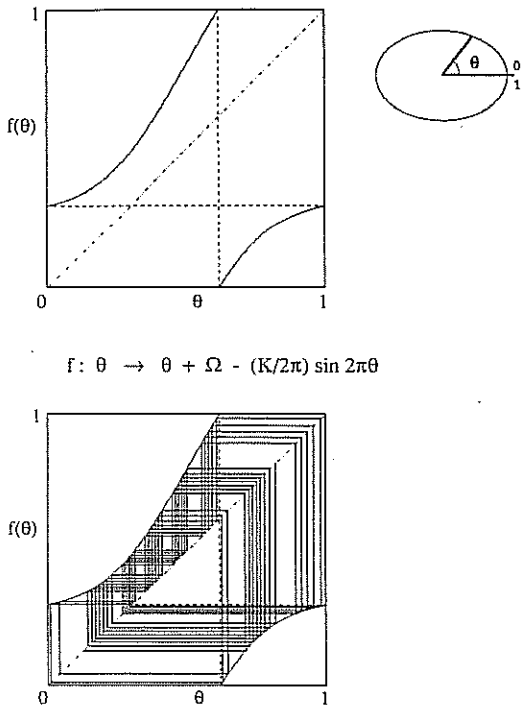

Figure 9. The standard circle or sine map. The sine map may be iterated in the same manner as the logistic map, by going up to the curve, reflecting in the 45° line, and going back to the curve.

map, let $f^n(\theta_0)$ represent the n^{th} iterate of the map, and consider the winding or rotation number:

$$W = \lim_{n\to\infty} \frac{f^n(\theta_0)-\theta_0}{n}. \tag{17}$$

The winding number, in effect, measures the average number of rotations per iterate. An orbit may converge to a series which is periodic (with period Q and rational rotation number $W=P/Q$), quasiperiodic (with irrational rotation number) or chaotic. In the latter instance, the series is erratic and the limit [equation (17)] fails to exist. For a suspended continuous-time system, the rotation number specifies the average number of system cycles per forcing cycle. If the underlying discrete-time orbit is periodic (with rotation number P/Q) the continuous-time system is said to be entrained or to exhibit Q:P phase locking.

The standard circle map contains two parameters: Ω sets the overall rate of rotation, whereas K is a measure of the nonlinearity in the system. The parameter K is critical in determining the shape of the sine map (Fig. 10). For

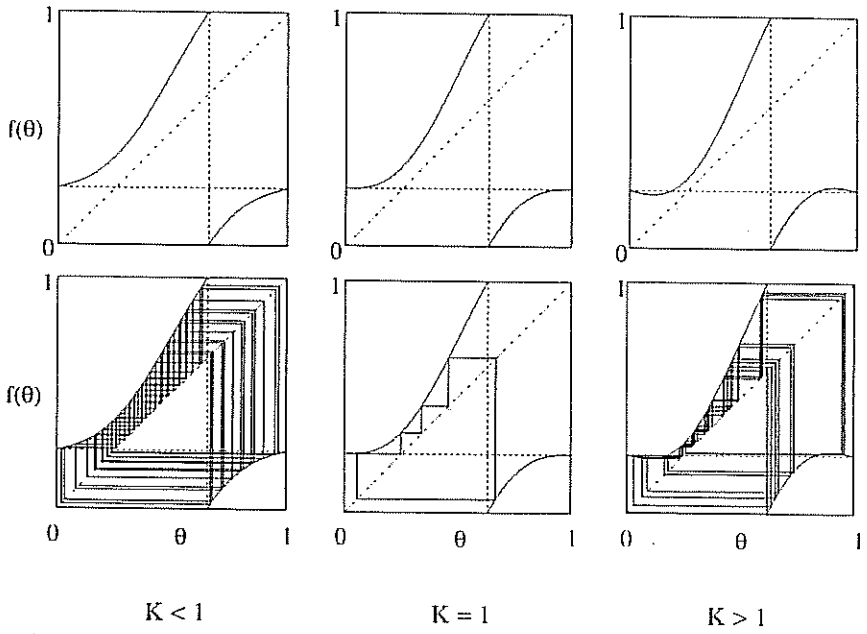

Figure 10. Effect of K on the shape and dynamics of the sine map. For $|K|<1$, the sine map is strictly monotonic (with 0 and 1 identified). At $K=1$, the map develops a cubic inflection. For $K>1$, the map develops a local maximum and minimum and is no longer invertible. Shown on the bottom are (left) quasiperiodic, (center) periodic, and (right) chaotic orbits.

$|K|<1$, the map is strictly monotonic. In particular, $f(\theta)$ and its inverse exist and are differentiable—$f(\theta)$ is a diffeomorphism. At $K=1$, the map develops a cubic inflection point and $f^{-1}(\theta)$ develops a singularity. For $K>1$, the map has both a local minimum and a local maximum and is no longer invertible.

The shape of the map dictates the prevailing dynamics. For each K, $0<K\leqslant 1$, and for each rational rotation number P/Q, one can find a finite nonzero interval in Ω wherein the iterated map achieves that rotation number. These phase-locking intervals form a series of cusped Arnol'd tongues in the Ω–K parameter plane (Fig. 11). As one enters an Arnol'd tongue—say of period 3—the graph of f^3 undergoes a tangent bifurcation (Fig. 12) and begets six fixed points: three intersections (those of shallow slope) constitute a stable three-cycle, the other three comprise an unstable three-cycle. The stable and unstable points diverge and then reconverge as one crosses the tongue; they are lost in a reverse tangent bifurcation as one exits the tongue. The existence of a stable three-cycle for the mapping implies the existence of a stable cycle of three times the forcing period for the corresponding continuous-time system.

For K close to zero, the tongues are narrow; one encounters irrational rotation numbers and quasiperiodicity rather frequently. Increasing K, the phase-locked intervals widen and periodic solutions pullulate. However, as

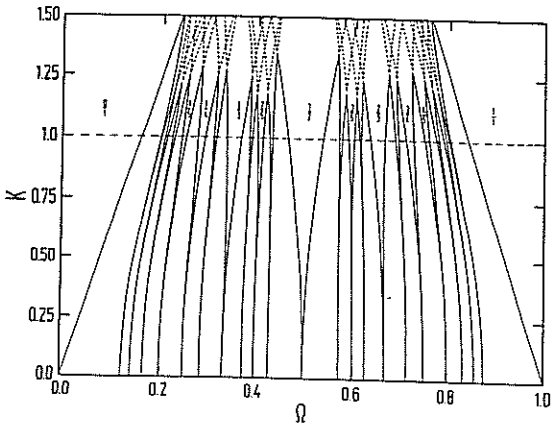

Figure 11. Arnol'd tongue diagram for the sine map. The more prominent phase-locked tongues or resonance horns of the sine map are shown in the Ω–K parameter plane. The tongues widen for increasing K and begin to overlap for $K>1$. The fractions indicate the winding or rotation number within each tongue. From Jensen *et al.* (1984).

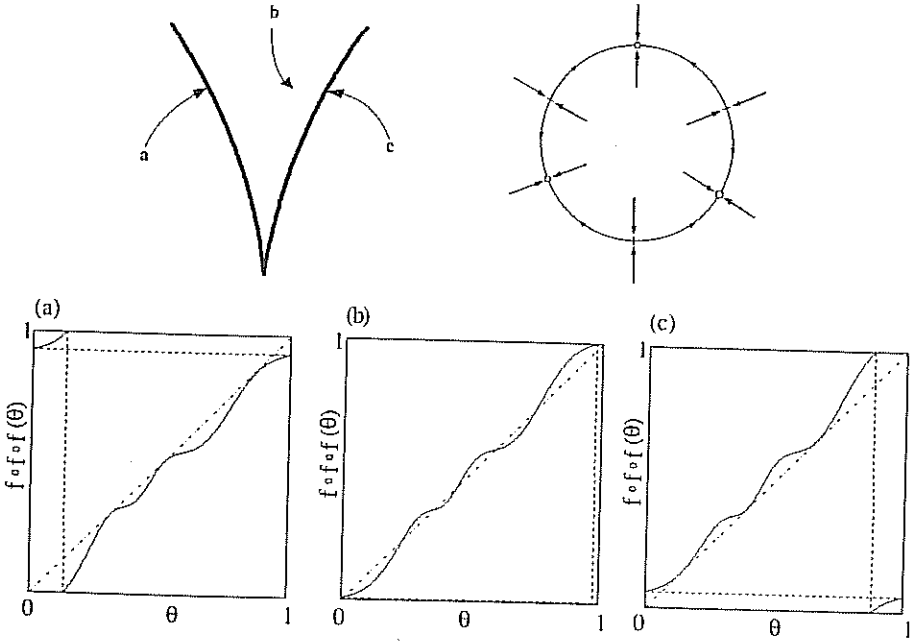

Figure 12. The origin and loss of period 3 frequency locking in the sine map. (a) As one enters a 3:1 resonance horn, the graph of $f^3(\theta)$ undergoes a tangent bifurcation. (b) A stable and an unstable three-cycle may coexist within the horn. The three fixed points of shallow slope constitute a stable three-cycle; the other three fixed points comprise the unstable three-cycle. (c) Upon leaving the Arnol'd tongue, the graph of $f^3(\theta)$ undergoes a reverse tangent bifurcation: the stable and unstable three-cycles collide and are annihilated.

long as $K\leqslant 1$, distinct tongues do not overlap and there is room for quasiperiodic orbits. As K nears one, the sine map acquires a horizontal tangent. Neighboring points are now drawn together (by a factor of $|df/d\theta|$ at each iterate) and phase-locking is forced upon the system. It has been shown numerically (Jensen *et al.*, 1983, 1984) that at the critical line $K=1$ the graph of winding number as a function of Ω forms a complete devil's staircase (Fig. 13). In effect, resonances completely fill the critical line, confining the quasiperiodic orbits to a Cantor set of measure zero and of fractal dimension $D\approx 0.87$.

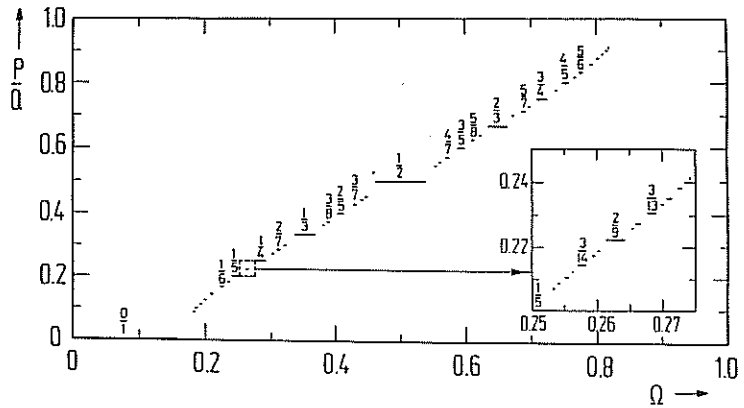

Figure 13. Devil's staircase for the sine map for $K=1$. The graph is a plot of the winding number W vs Ω. The steps are the regions in which the W is constant and rational. They are, in effect, slices through the resonance horns. At $K=1$, the staircase is complete; the resonances fill the line, confining quasiperiodic orbits to a set of measure zero. From Schuster (1988) after Jensen *et al.* (1984).

For $K>1$, the map $f(\theta)$ is no longer invertible. It has, in fact, developed quadratic maxima and minima. In the neighborhood of each extremum, the circle map recapitulates the properties of a simple unimodal map such as the logistic difference equation. Globally, its behavior is more analogous to a simple bimodal cubic or quartic map (May, 1979, 1980b; Chang *et al.*, 1981, 1982; Schell *et al.*, 1983; Skjolding *et al.*, 1983; Kot and Schaffer, 1984). In either instance, a simple periodic solution may now lose its stability in a cascade of period-doubling bifurcations. Consider, for example, a three-cycle (Fig. 14): there are three stable ($|df^3/d\theta|<1$) fixed points for $K<1$, but these three may lose their stability ($df^3/d\theta<-1$) for $K>1$. Period-doubling cascades are nested within Arnol'd tongues: a P/Q cycle may give rise to $2P/2Q$, $4P/4Q$, $8P/8Q$ ... cycles, all with a constant winding number. Complete cascades give rise to chaotic dynamics but chaotic dynamics may also appear by intermittency or via global bifurcations (Schell *et al.*, 1983; MacKay and Tresser, 1984; Thompson and Stewart, 1986). In the Ω–K plane, Arnol'd

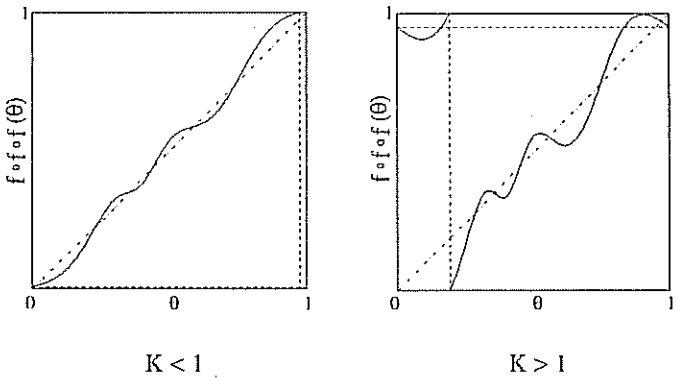

Figure 14. Deformation of $f^3(\theta)$ with an increase in K. Inside the 3:1 resonance horn and for (left) $K<1$, $f^3(\theta)$ has a stable and an unstable three-cycle. For (right) $K>1$, the first of these three-cycles may also lose its stability ($df^3/d\theta<-1$) as $f^3(\theta)$ develops maxima and minima. With the loss of stability we observe one or more period-doubling bifurcations. Period-doubling cascades occur nested within the Arnol'd tongues.

tongues overlap, leading to bistability, multistability, and the potential for hysteresis.

Although we have concentrated on the standard circle map [equation (16)], our discussion does not rely critically on the use of the function sin $(2\pi\theta)$. Virtually any function with a single cubic inflection point will yield the same qualitative and similar quantitative behavior. Armed with this universality, we may now return to the forced double-Monod system with some reasonable idea of what may happen.

5. The Forced Double-Monod System Revisited. The forced double-Monod system harbors circle maps (see Fig. 7). We have already seen that circle maps may possess critical curves, the locus of points in parameter space at which the circle map loses invertibility, and that these curves are important harbingers. For the sine map, the critical curve ($K=1$) was especially simple. We do not expect such simplicity in our chemostat system. Nevertheless, we may still hope for a critical curve.

It is convenient to look for phase locking and criticality in the two-dimensional T–ε parameter space, where T is the period and ε is the amplitude of forcing [see equation (9)]. For the sine map, Ω set the overall rate of rotation, whereas K was a measure of the nonlinearity in the system. For the forced double-Monod system, the situation is more complicated. Both ε and T affect the amplitude of the simplex vibration [equation (15)]; it might be imagined that an increase in either will lead to criticality, period doubling, and chaos. This is indeed the case!

Let us begin, as before, with the physiological parameters of Table 2, an with the chemostat parameters set to $S_i=115$ mg l^{-1} and $D=0.1$ h^{-1}; thes are values that give rise to a simple limit cycle (Fig. 3) of period just over 47 ($\tau\approx4.73$) in the absence of forcing. If we allow small-amplitude ($\varepsilon=0.1$) forcin for a range of forcing periods T, we may produce the bifurcation diagrar illustrated in Fig. 15. This diagram, obtained by stroboscopically samplin

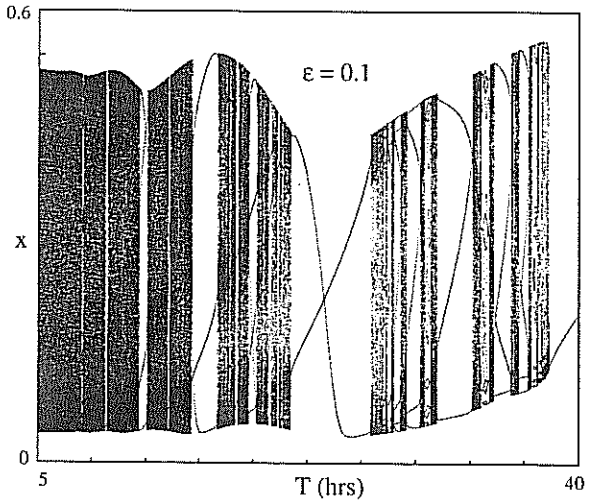

Figure 15. Bifurcation diagram for the forced double-Monod model for $\varepsilon=0.1$, variable T, and all other parameters as in Fig. 3. The diagram is constructed by stroboscopically sampling the rescaled substrate concentration x at the forcing period (or at DT in rescaled time) for each of 1 000 forcing periods T. For each T, 400 samples were plotted after a transient of 150 strobes. Because we sample a single variable, quasiperiodic solutions appear as intervals of points; n-cycles appear as n distinct points. Phase locking and period doubling are increasingly common with increasing T.

dimensionless substrate [equation (10)] at multiples of DT, illustrates th asymptotic behavior of the system along a slice in the T–ε plane. By samplin just one variable, we project the attractor (for each T) down onto on dimension: quasiperiodic invariant circles appear as an interval of point simple n-cycles appear as n distinct points. For small forcing periods T quasiperiodic solutions predominate. As we increase T, phase locking become more apparent and phase-locking intervals widen. Looking closely at the righ of Fig. 15, we observe, for higher T, a number of phase-locking intervals i which a single period doubling takes place. In Fig. 16, we plot the rationa rotation numbers for the more prominent phase-locking regions of Fig. 15. Fo small T, phase-locking intervals are rather narrow. As we increase T, the devil' staircase is noticeably more complete—it does a better job of covering the axis. All of these trends are hallmarks of criticality.

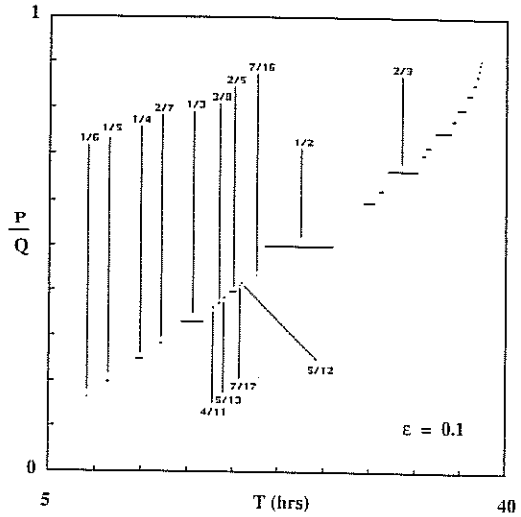

Figure 16. Devil's staircase for the forced double-Monod system for $\varepsilon=0.1$. The graph is a plot of the winding number W vs T. The steps are the regions in which W is constant and rational. They are, in effect, slices through the resonance horns. The staircase becomes progressively more complete as T increases.

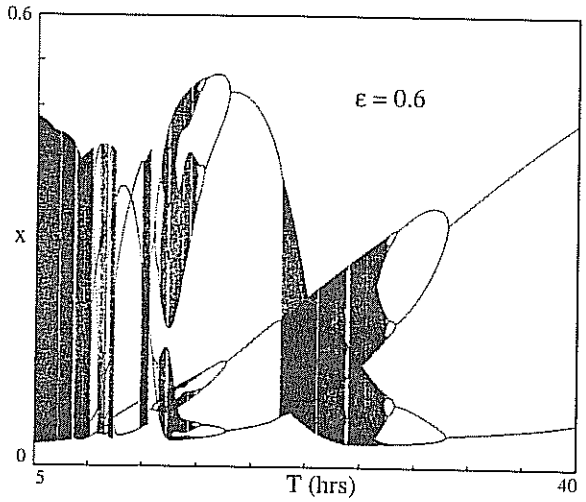

Figure 17. Bifurcation diagram for the forced double-Monod system for $\varepsilon=0.6$, variable T, and all other parameters as in Fig. 3. The diagram is constructed as in Fig. 15. At this intermediate amplitude of forcing, all the bellweathers of criticality are accentuated: phase-locking intervals appear sooner and are wider; period doubling also begins sooner and progresses further.

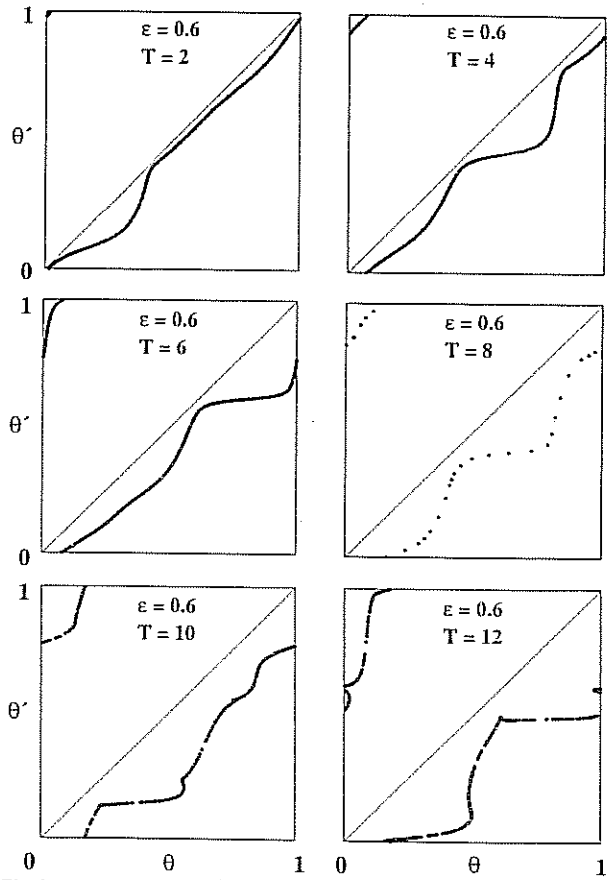

Figure 18. Circle maps for the forced double-Monod system for $\varepsilon=0.6$. There is a marked tendency toward criticality in the map with increasing T.

At an intermediate amplitude ($\varepsilon=0.6$), all of these trends are accentuated (Fig. 17). The interval in T for which quasiperiodic orbits predominate is narrower, phase-locking intervals are substantially wider, period-doubling begins sooner and progresses further. Indeed, Fig. 17 shows fairly complete period-doubling cascades. Chaotic solutions commonly occur at the end of these cascades; the strange attractor of Fig. 6 arises after one such cascade. Stronger evidence for criticality comes from a direct computation of the first return map. Figure 18 shows Poincaré maps for $\varepsilon=0.6$ and a range of T values. There is a progressive levelling of the circle map culminating in a map that is nearly flat at $T=12$. This leveling occurs just before the first period-doubling cascade in Fig. 17.

By combining bifurcation diagrams for a large number of amplitudes and for various initial conditions, we have put together a two-dimensional T–ε control diagram (Fig. 19). The diagram is incomplete, but does show the most

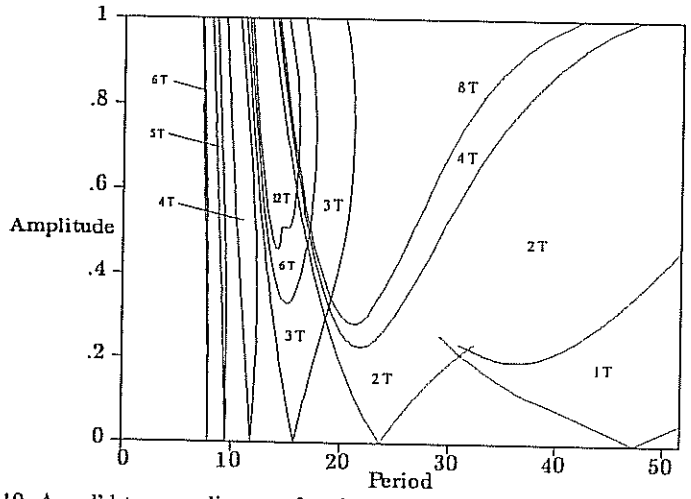

Figure 19. Arnol'd tongue diagram for the forced double-Monod system with all other parameters as in Fig. 3. The more prominent phase-locked tongues or resonance horns of the forced double-Monod system are shown in the T–ε parameter plane. The tongues widen for increasing T and begin to overlap for high T and ε. The numbers represent the observed periods within the tongues as multiples of the forcing period T. Period-doubling cascades may be observed for high T and ε. This diagram was constructed by brute-force assimilation of a large number of bifurcation diagrams (cf Figs 15 and 17).

rominent phase-locking regions (Arnol'd tongues). These tongues widen with n increase in forcing period T and, at least initially, with an increase in forcing mplitude ε. The 3:1, 2:1 and 1:1 resonance horns splay with such rapidity that hey overlap throughout much of the control diagram. In these regions of verlap the system exhibits bistability or multistability: two or more stable eriodic solutions and/or strange attractors coexist. There appear to be global ifurcations that complicate the overlap of the 2:1 and 1:1 resonance horns. Nestled within several of the horns are cascades of period-doubling ifurcations. Relatively few of the period-doubling bifurcations are actually hown in Fig. 19, but it is clear that they occur for high T and ε.

Figures 20 and 21 demonstrate that the resonance horns arise as tangent ifurcations of an iterated circle map. Figure 20 illustrates the third-composite rcle map for small amplitude ($\varepsilon = 0.05$) and a range of forcing periods T. [The orresponding Poincaré sections were obtained by sampling system (10) at ıultiples of $3DT$.] This map, quite distant from the 45° line for small T, rapidly pproaches this line as we increase T. Tangency occurs as we cross the left oundary of the 3:1 resonance horn in Fig. 19. It is apparent from the shape of ıe map, that the bifurcation will yield one stable and one unstable three-cycle. we examine the fourth-composite circle map (Fig. 21) at an intermediate mplitude ($\varepsilon = 0.6$), we again observe a tangent bifurcation, coincident with our

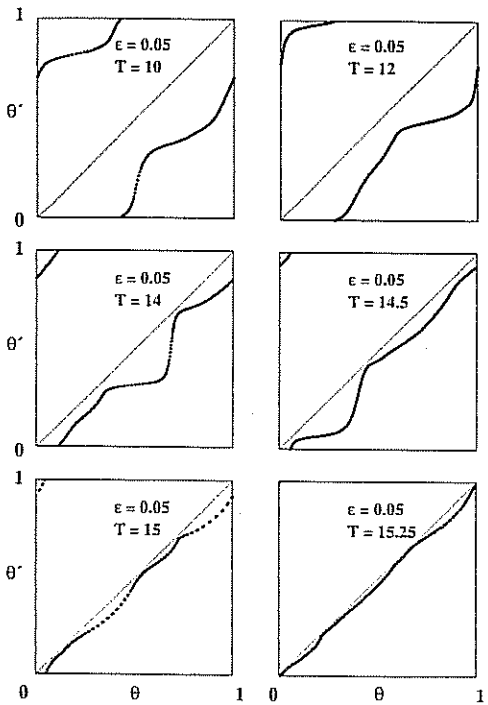

Figure 20. The origin of period 3 frequency locking in the forced double-Monod system for $\varepsilon = 0.05$. The figure illustrates the third-composite circle map for small amplitude and a range of forcing periods T. A tangent bifurcation, yielding a stable and an unstable three-cycle, occurs as the map approaches the 45° line. The base parameters are identical to those in Fig. 3.

crossing the left boundary of the 4:1 resonance horn. This fourth-composit map is already remarkably close to criticality.

6. Conclusions. The patterns we have found are robust. We have examine the forced double-Monod system for an assortment of parameter values: circl maps continually arise from forced limit cycles. In addition, we consistentl observe a route to chaos:

quasiperiodicity→phase locking→period doubling→chaos

that is characteristic of simple circle maps. Our search of parameter space ha not, however, been exhaustive: more complicated maps and scenarios (cf Ruelle and Takens, 1971; Kaneko, 1986) could conceivably occur.

What of variation in the actual differential equations? For small changes, we once again, expect indifference to detail. Our discussion of circle maps did no rely critically on the use of the function sin $(2\pi\theta)$. Virtually any function with a single cubic inflection point yields the same qualitative and similar quantitativ behavior. Likewise, the mode-locking route to chaos is typical of an entire clas

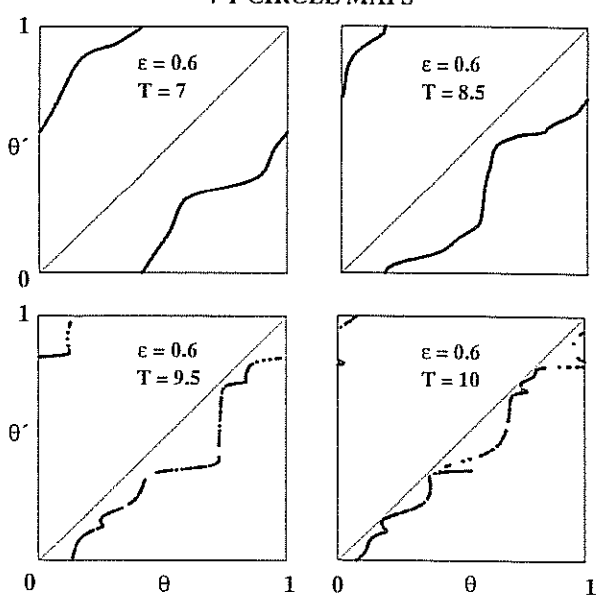

Figure 21. The origin of period 4 frequency locking in the forced double-Monod system for $\varepsilon=0.6$. The figure illustrates the fourth-composite circle map for intermediate amplitude and a range of forcing periods T. A tangent bifurcation, yielding a stable and an unstable four-cycle, occurs as the map approaches the 45° line. This circle map is already remarkably close to criticality. The base parameters are identical to those in Fig. 3.

of differential equations—those with two competing frequencies. If a chemostat can support a limit cycle in the absence of forcing, forcing should yield phase locking, and, given a large enough amplitude or period of forcing, a phase-locking route to chaos.

For biologists, the verity and significance of the last statement must be gauged experimentally. For this reason, we have initiated continuous co-culture of *Tetrahymena pyriformis* and *Escherichia coli* on a glucose substrate. Our goal is to test the predictions of the forced double-Monod model. It is interesting that circle maps appear even here: chemostats are subject to what is often sizable experimental noise. This noise may obscure certain characteristics of chaos, most notably sensitive dependence on initial conditions and period doubling. In contrast, numerical experiments (Schaffer *et al.* 1988) suggest that circle maps may retain their essential form even in the presence of substantial noise. Circle maps may thus play as essential a role in assessing data as in developing theory.

One may easily imagine substrates other than glucose. Indeed, there is tremendous wordwide interest in bioremediation, wherein microbes facilitate the biodegradation of xenobiotics and other pollutants (Omenn, 1988). If a

xenobiotic substrate is forced into a chemostat with a predator and biodegrading prey, details of the population dynamics will surely affect the rat and effectiveness of bioremediation. Chaos would then be of profoun practical, as well as intrinsic, interest.

We wish to thank William Schaffer for his helpful comments and Celeste A Berg for her careful reading of the manuscript. M.K. wishes to acknowledge th Department of Energy (DE-FG06-90ER61034) and the National Scienc Foundation (BSR-8907965) for their support.

LITERATURE

Alexander, M. 1981. Why microbial predators and parasites do not eliminate their prey an hosts. *Ann. Rev. Microbiol.* **35**, 113–133.

Allen, J. 1990. Chaos and phase-locking in predator–prey models in relation to the function response. *Florida Ent.* **73**, 100–110.

Arnol'd, V. I. 1965. Small denominators, I. Mappings of the circumference onto itself. *Am. mat Soc. Transl.* **46**, 213–284.

Andronov, A. A., E. A. Vitt and S. E. Khaiken. 1966. *Theory of Oscillators*. Oxford: Pergamc Press.

Bak, P. 1986. The devil's staircase. *Phys. Today* **39**, 38–45.

Bazin, M. J., C. Curds, A. Dauppe, B. A. Owen and P. T. Saunders. 1983. Microbial predatic dynamics. *ACS Symposium Series* **207**, 253–264.

Bellows, T. S. 1981. The descriptive properties of some models for density dependence. *J. anir Ecol.* **50**, 139–156.

Berryman, A. A. and J. A. Millstein. 1989. Are ecological systems chaotic—and if not, why no *Trends Ecol. Evol.* **4**, 26–28.

Butler, G. J., S. B. Hsu and P. Waltman. 1983. Coexistence of competing predators in chemostat. *J. math. Biol.* **17**, 133–151.

Canale, R. P. 1970. An analysis of models describing predator–prey interaction. *Biotec Bioengng* **12**, 353–378.

Canale, R. P., T. D. Lustig, P. M. Kehrberger and J. E. Salo. 1973. Experimental an mathematical modeling studies of protozoan predation on bacteria. *Biotech. Bioengng* **1** 707–728.

Caswell, H. and D. E. Weeks. 1986. Two-sex models: chaos, extinction, and other dynam consequences of sex. *Am. Nat.* **128**, 707–735.

Chang, S.-J., M. Wortis and J. A. Wright. 1981. Iterative properties of a one-dimensional quart map: Critical lines and tricritical behavior. *Phys. Rev. A.* **24**, 2669–2694.

Chang, S.-J., M. Wortis and J. A. Wright. 1982. Tricritical points and bifurcations in the quart map. In *Nonlinear Problems: Present and Future*, A. R. Bishop and D. K. Campbell (Eds pp. 395–402. Amsterdam: North-Holland.

Collet, P. and J. P. Eckmann. 1980. *Iterated Maps on the Interval as Dynamical Systems*. Base Birkhauser.

Contois, D. E. 1959. Kinetics of bacterial growth: relationship between population density an specific growth rate of continuous cultures. *J. gen. Microbiol.* **33**, 40–50.

Cunningham, A. and R. M. Nisbet. 1983. Transients and oscillations in continuous culture. I *Mathematics in Microbiology*, M. Bazin (Ed.), pp. 77–103. London: Academic Press.

Curds, C. R. and A. Cockburn. 1968. Studies on the growth and feeding of *Tetrahymen pyriformis* in axenic and monoxenic culture. *J. gen. Microbiol.* **54**, 343–358.

Curds, C. R. and M. J. Bazin. 1977. Protozoan predation in batch and continuous culture. *Ad aquat. Microbiol.* **1**, 115–176.

Dent, V. E., M. J. Bazin and P. T. Saunders. 1976. Behaviour of *Dictyostelium discoideum* amoebae and *Escherichia coli* grown together in a chemostat culture. *Arch. Microbiol.* **109**, 187–194.
Devaney, R. L. 1986. *An Introduction to Chaotic Dynamical Systems*. Menlo Park: Benjamin/Cummings.
Drake, J. F. and H. M. Tsuchiya. 1976. Predation on *Escherichia coli* by *Colpoda steinii*. *Appl. environ. Microbiol.* **331**, 870–874.
Drake, J. F. and H. M. Tsuchiya. 1977. Growth kinetics of *Colpoda steinii* on *Escherichia coli*. *Appl. environ. Microbiol.* **34**, 18–22.
Farmer, J. D. 1985. Sensitive dependence on parameters in nonlinear dynamics. *Phys. Rev. Lett.* **55**, 351–354.
Feigenbaum, M. 1978. Quantitative universality for a class of nonlinear transformations. *J. stat. Phys.* **19**, 25–52.
Feigenbaum, M. 1979. Universal metric properties of nonlinear transformations. *J. stat. Phys.* **21**, 669–706.
Feigenbaum, M. 1983. Universal behavior in nonlinear systems. *Physica D* **7**, 16–39.
Fredrickson, A. G. 1983. Interactions of microbial populations in mixed culture situations. *ACS Symposium Series* **207**, 201–227.
Gilpin, M. E. 1979. Spiral chaos in a predator–prey model. *Am. Nat.* **113**, 306–308.
Glazier, J. A. and A. Libchaber. 1988. Quasi-periodicity and dynamical systems: an experimentalist's view. *IEEE Trans. Circ. Syst.* **35**, 790–809.
Graham, J. M. and R. P. Canale. 1982. Experimental and modeling studies of a four-trophic level predator–prey system. *Microb. Ecol.* **8**, 217–232.
Grebogi, C., E. Ott and J. A. Yorke. 1983. Crises, sudden changes in chaotic attractors, and transient chaos. *Physica D* **7**, 181–200.
Hassell, M. P., J. H. Lawton and R. M. May. 1976. Patterns of dynamical behavior in single-species populations. *J. anim. Ecol.* **45**, 471–486.
Hastings, A. and T. Powell. 1992. Chaos in a three species food chain. *Ecology*, in press.
Holling, C. S. 1959. Some characteristics of simple types of predation and parasitism. *Can. Ent.* **91**, 385–395.
Inoue, M. and H. Kamifukumoto. 1984. Scenarios leading to chaos in a forced Lotka–Volterra model. *Prog. theor. Phys.* **71**, 930–937.
Jacobson, M. V. 1981. Absolutely continuous invariant measure for one-parameter families of one-dimensional maps. *Communs Math. Phys.* **81**, 39–88.
Jensen, M. H., P. Bak and T. Bohr. 1983. Complete devil's staircase, fractal dimension, and universality of mode-locking structure in the circle map. *Phys. Rev. Lett.* **50**, 1637–1639.
Jensen, M. H., P. Bak and T. Bohr. 1984. Transition to chaos by interaction of resonances in dissipative systems. I. Circle maps. *Phys. Rev. A* **30**, 1960–1969.
Jost, J. L., J. F. Drake, A. G. Fredrickson and J. M. Tsuchiya. 1973. Interactions of *Tetrahymena pyriformis, Escherichia coli, Azotobacter vinelandii*, and glucose in a minimal medium. *J. Bacteriol.* **113**, 834–840.
Kaneko, K. 1986. *Collapse of Tori and Genesis of Chaos in Dissipative Systems*. Singapore: World Scientific.
Kot, M. and W. M. Schaffer. 1984. The effects of seasonality on discrete models of population growth. *Theoret. popul. Biol.* **26**, 340–360.
Kot, M. and W. M. Schaffer. 1986. Discrete-time growth-dispersal models. *Math. Biosci.* **80**, 109–136.
Kot, M., W. M. Schaffer, G. L. Truty, D. J. Graser and L. F. Olsen. 1988. Changing criteria for imposing order. *Ecol. Mod.* **43**, 75–110.
Kuang, Y. 1989. Limit cycles in a chemostat-related model. *SIAM J. appl. Math.* **49**, 1759–1767.
Leven, R. W., B. P. Kock and G. S. Markman. 1987. Periodic, quasiperiodic, and chaotic motion in a forced predator–prey ecosystem. In *Dynamical Systems and Environmental Models*, H. G. Bothe, W. Ebeling, A. B. Kurzhanski and M. Peschel (Eds), pp. 95–104. Berlin: Akademie-Verlag.
Li, T. Y. and J. A. Yorke. 1975. Period three implies chaos. *Am. math. Mon.* **82**, 985–992.

May, R. M. 1972. On relationships among various types of population models. *Am. Nat.* **107** 46–57.
May, R. M. 1974. Biological populations with nonoverlapping generations: stable points, stabl cycles, and chaos. *Science* **186**, 645–647.
May, R. M. 1976. Simple mathematical models with very complicated dynamics. *Nature* **261** 459–467.
May, R. M. and G. F. Oster. 1976. Bifurcations and dynamic complexity in simple ecologica models. *Am. Nat.* **110**, 573–599.
May, R. M. 1979. Bifurcations and dynamic complexity in ecological systems. *Annls. N.Y. Acad Sci.* **316**, 517–529.
May, R. M. 1980a. Mathematical models in whaling and fisheries management. In *Som Mathematical Questions in Biology*, Vol. 13, G. F. Oster (Ed.), pp. 1–64. Providence Mathematical Society.
May, R. M. 1980b. Nonlinear phenomena in ecology and epidemiology. *Annls. N.Y. Acad. Sci.* **357**, 282–291.
May, R. M. 1985. Regulation of populations with non-overlapping generations by micropara sites: a purely chaotic system. *Am. Nat.* **125**, 573–584.
Maynard Smith, J. 1968. *Mathematical Ideas in Biology*. Cambridge, U.K.: Cambridg University Press.
MacKay, R. S. and C. Tresser. 1984. Transition to chaos for two-frequency systems. *J. Phys Lett.* **44**, L741–L746.
Metropolis, N., M. L. Stein and P. R. Stein. 1973. On finite limit sets of transformations on th unit interval. *J. Comb. Theor.* **15**, 25–44.
Monod, J. 1942. *Recherches sur la Croissance des Cultures Bacteriennes*. Paris: Hermann.
Monod, J. 1950. La technique de culture continue; theorie et application. *Annls Inst. Pasteur* 79 390–401.
Nisbet, R. M., A. Cunningham and W. S. C. Gurney. 1983. Endogenous metabolism and th stability of microbial predator–prey systems. *Biotech. Bioengng* **25**, 301–306.
Olsen, L. F. 1987. Low dimensional strange attractors in epidemics of childhood diseases i Copenhagen, Denmark. In *Chaos in Biological Systems*, H. Degn, A. V. Holden and L. F Olsen (Eds), NATO ASI Series, Series A, Vol. 138. New York: Plenum.
Olsen, L. F., W. M. Schaffer and G. L. Truty. 1988. Oscillations and chaos in epidemics: nonlinear dynamics study of six childhood diseases in Copenhagen, Denmark. *Theor. Popu Biol.* **33**, 344–370.
Olsen, L. F. and W. M. Schaffer. 1990. Chaos versus noisy periodicity: alternative hypotheses fo childhood epidemics. *Science* **249**, 499–504.
Omenn, G. S. 1988. *Environmental Biotechnology—Reducing Risks from Environmentc Chemicals Through Biotechnology*. New York: Plenum Press.
Poincaré, H. 1892. *Les Méthodes Nouvelles de la Méchanique Celeste*. Paris: Gauthier-Villars
Pool, R. 1989a. Is it chaos, or is it just noise? *Science* **243**, 25–28.
Pool, R. 1989b. Ecologists flirt with chaos. *Science* **243**, 310–313.
Press, W. H., B. P. Flannery, S. A. Teukolsky and W. T. Vetterling. 1988. *Numerical Recipes in C* Cambridge: Cambridge University Press.
Proper, G. and J. C. Garver. 1966. Mass culture of the protozoa *Colpoda steinii*. *Biotechno Bioengng* **8**, 287–296.
Ratnam, D. A., S. Pavlou and A. G. Fredrickson. 1982. Effects of attachment of bacteria t chemostat walls in a microbial predator–prey relationship. *Biotech. Bioengng* **24**, 2675–269
Ricker, W. E. 1954. Stock and recruitment. *J. Fish. Res. Bd Can.*, **11**, 559–623.
Rodgers, T. D. 1981. Chaos in systems in population biology. *Prog. theor. Biol.* **6**, 91–146.
Rosenzweig, M. L. 1971. Paradox of enrichment: destabilization of exploitation ecosystems i ecological time. *Science* **171**, 385–387.
Ruelle, D. and F. Takens. 1971. On the nature of turbulence. *Communs math. Phys.* **20**, 167–192
Salt, G. W. 1967. Predation in an experimental protozoa population (*Woodruffia–Paramecium Ecol. Monogr.* **37**, 113–144.

Sarkovskii, A. N. 1964. Coexistence of cycles of a continuous map of a line into itself. *Ukr. mat. Zh.* **16**, 61–71.
Schaffer, W. M. 1985. Can nonlinear dynamics elucidate mechanisms in ecology and epidemiology? *IMA J. Math. appl. med. Biol.* **2**, 221–252.
Schaffer, W. M. and M. Kot. 1985. Nearly one dimensional dynamics in a simple epidemic. *J. theor. Biol.* **112**, 403–427.
Schaffer, W. M. 1989. Perceiving order in the chaos of nature. In *Evolution of Life Histories*. M. Boyce (Ed.), pp. 313–350. New Haven: Yale University Press.
Schaffer, W. M. and M. Kot. 1986a. Differential systems in ecology and epidemiology. In *Chaos*, A. V. Holden (Ed.), pp. 158–178. Princeton: Princeton University Press.
Schaffer, W. M. and M. Kot. 1986b. Chaos in ecological systems: the coals that Newcastle forgot. *Trends Ecol. Evol.* **1**, 58–63.
Schaffer, W. M., L. F. Olsen, G. L. Truty, S. L. Fulmer and D. J. Graser. 1988. Periodic and chaotic dynamics in childhood infections. In *From Chemical to Biological Organization*. M. Markus, S. Muller and G. Nicolis (Eds), pp. 331–347. Berlin: Springer.
Schell, M., S. Fraser and R. Kapral. 1983. Subharmonic bifurcation in the sine map: An infinite hierarchy of cusp bistabilites. *Phys. Rev. A* **28**, 373–378.
Schuster, H. G. 1988. *Deterministic Chaos: An Introduction*. Weinheim: VCH.
Skjolding, H., B. Branner-Jorgensen, P. L. Christiansen and H. E. Jensen. 1983. Bifurcations in discrete dynamical systems with cubic maps. *SIAM J. appl. Math.* **43**, 520–534.
Stefan, P. 1977. A theorem of Sarkovskii on the existence of periodic orbits of continuous endomorphisms of the real line. *Communs Math. Phys.* **54**, 237—248.
Stubbs, M. 1977. Density dependence in the life-cycles of animals and its importance in *K* and *r*-strategies. *J anim. Ecol.* **46**, 677–688.
Sudo, R., K. Kobayashi and S. Aiba. 1975. Some experiments and analysis of a predator–prey model: Interaction between *Colpidium campylum* and *Alcaligenes faecalis* in continuous and mixed culture. *Biotech. Bioengng.* **17**, 167–184.
Swift, S. T., I. Y. Najita, K. Ohtaguchi and A. G. Fredrickson. 1982a. Continuous culture of the ciliate *Tetrahymena pyriformis* on *Escherichia coli*. *Biotech. Bioengng* **24**, 1953–1964.
Swift, S. T., I. Y. Najita, K. Ohtaguchi and A. G. Fredrickson. 1982b. Some physiological aspects of the autecology of the suspension-feeding protozoan *Tetrahymena pyriformis*. *Microb. Ecol.* **8**, 201–215.
Takens, F. 1981. Detecting strange attractors in turbulence. *Lect. Notes Math.* **898**, 366–381.
Taylor, W. D., M. A. Gates and J. Berger. 1976. Morphological changes during the growth cycle of axenic and monoxenic *Tetrahymena pyriformis*. *Can. J. Zool.* **54**, 2011–2018.
Thomas, W. R., M. J. Pomerantz and M. E. Gilpin. 1980. Chaos, asymmetric growth, and group selection for dynamical stability. *Ecology* **61**, 1312–1320.
Thompson, J. M. T. and Stewart, H. B. 1986. *Nonlinear Dynamics and Chaos*. Chichester: Wiley.
Tsuchiya, H. M., J. F. Drake, J. L. Jost and A. G. Fredrickson. 1972. Predator–prey interactions of *Dictyostelium discoideum* and *Escherichia coli* in continuous culture. *J. Bacteriol.* **110**, 1147–1153.
van den Ende, P. 1973. Predator–prey interactions in continuous culture. *Science* **181**, 562–564.
Varon, M. and B. P. Zeigler, 1978. Bacterial predator–prey interaction at low prey density. *Appl. environ. Microbiol.* **36**, 11–17.
Waltman, P. 1983. *Competition Models in Population Biology*. Philadelphia: Society for Industrial and Applied Mathematics.
Watson, P. J., O. Kazuhisa and A. G. Fredrickson. 1981. Kinetics of growth of the ciliate *Tetrahymena pyriformis* on *Escherichia coli*. *J. gen. Microbiol.* **122**, 323–333.

Received 26 October 1990
Revised 3 March 1991

Bulletin of Mathematical Biology Vol. 54, No. 4, pp. 649–672, 1992.
Printed in Great Britain.

0092-8240/92$5.00 + 0.
Pergamon Press p
Society for Mathematical Biolo

MODELING IMMUNE REACTIVITY IN SECONDARY LYMPHOID ORGANS*

■ ALAN S. PERELSON
Theoretical Division,
Los Alamos National Laboratory,
Los Alamos, NM 87545, U.S.A.
(*E.mail: asp@receptor.lanl.gov*)

■ GÉRARD WEISBUCH
Laboratorie de Physique Statistique,
l'Ecole Normale Supérieure,
24 rue Lhomond, F 75231,
Paris Cedex 5, France
(*E.mail: weisbuch@FRULM62.bitnet*)

Models of the dynamical interactions important in generating immune reactivity have generall assumed that the immune system is a single well-stirred compartment. Here we explicitly tak into account the compartmentalized nature of the immune system and show that qualitativ conclusions, such as the stability of the immune steady state, depend on architectural details. W examine a simple model idiotypic network involving only two types of B cells and antibod molecules. We show, for model parameters used by De Boer *et al.* (1990, *Chem. Eng. Sci.* 4 2375–2382), that the immune steady state is unstable in a one compartmental model but stable i a two compartment model that contains both a lymphoid organ, such as the spleen, and th circulatory system.

Introduction. The immune system, which has the task of surveying the bod for the presence of foreign organisms, is of necessity a system distributec throughout the body. The system is composed of the primary lymphoid organs the bone marrow and the thymus, where B and T lymphoctyes are produced and a collection of secondary lymphoid organs, where immune responses ar initiated. The secondary lymphoid organs include the spleen, the lymph nodes the adenoids, the tonsils, the Peyer's patches of the small intestine and th appendix (cf. Jerne, 1973). The secondary lymphoid organs are connected b both the bloodstream and a system of small lymphatic vessels. Lymphocyte can enter these organs and either reside there or transit further into th surrounding tissues by moving through the lymph, the fluid bathing the cells o the body. The lymphatic system is composed of a widely dispersed network o thin-walled vessels with one-way valves and interspersed filtering organs, th lymph nodes. The lymphatics originate in the interstitial spaces of the tissues

* This work was performed under the auspices of the U.S. Department of Energy.